Received 26 October 2018
Revised 7 December 2018
Accepted 19 December 2018

Fluid-structure interaction analysis of transient convection heat transfer in a cavity containing inner solid cylinder and flexible right wall

Ammar I. Alsabery, Habibis Saleh, Mohammad Ghalambaz, Ali J. Chamkha and Ishak Hashim
(Author affiliations can be found at the end of the article)

Abstract

Purpose – This paper aims to investigate the fluid structure interaction analysis of conjugate natural convection in a square containing internal solid cylinder and flexible right wall.

Design/methodology/approach – The right wall of the cavity is flexible, which can be deformed due to the interaction with the natural convection flow in the cavity. The top and bottom walls of the cavity are insulated while the right wall is cold and the left wall is partially heated. The governing equations for heat, flow and elastic wall, as well as the grid deformation are written in Arbitrary Lagrangian–Eulerian formulation. The governing equations along with their boundary conditions are solved using the finite element method.

Findings – The results of the present study show that the presence of the solid cylinder strongly affects the transient solution at the initial times. The natural convection flow changes the shape of the flexible right wall of the cavity into *S* shape wall due to the interaction of the flow and the structure. It is found that the increase of the flexibility of the right wall increases the average Nusselt number of the hot wall up to 2 per cent.

Originality/value – To the best of the authors' knowledge, the unsteady natural convection in an enclosure having a flexible wall and inner solid cylinder has never been reported before.

Keywords Transient natural convection, Finite element method, Fluid-structure interaction, Elastic wall, Inner solid cylinder, Local isothermal heater

Paper type Research paper

Nomenclature

C_p = specific heat capacity;
$\mathbf{d}_s$ = displacement vector;
E = dimensionless elasticity modulus;
E_τ = dimensional Young's modulus;
F_ν = body force vector;
$\overrightarrow{g}$ = gravitational acceleration;
k = thermal conductivity;
K_r = thermal conductivity ratio;
L = width and height of cavity;

The work was supported by the grant GSP/1/2015/SG04/UKM/01/1.

International Journal of Numerical Methods for Heat & Fluid Flow
Vol. 29 No. 10, 2019
pp. 3756-3780

0961-5539
DOI 10.1108/HFF-10-2018-0593

$\overline{Nu}$ = average Nusselt number;
Pr = Prandtl number;
r and R = radius of inner cylinder and dimensionless radius of inner cylinder;
Ra = Rayleigh number;
t = dimensional time;
t_P = dimensionless thickness of the flexible wall;
t_p^* = dimensional thickness of the flexible wall;
T = temperature;
$\mathbf{u}$ = velocity vector;
u, v = dimensionless components of $\mathbf{u}$ in the X-direction and Y-direction;
x, y and X, Y = space coordinates and dimensionless space coordinates;
$\mathbf{w}$ = moving coordinate velocity; and
W_s = strain energy density function.

Greek symbols

α = thermal diffusivity;
α_r = thermal diffusivity ratio;
β = thermal expansion coefficient;
ε = strain;
θ = dimensionless temperature;
λ = Lame's first constant;
μ = dynamic viscosity;
μ_l = Lame's second constant;
ν = Poisson's ratio;
ν_f = kinematic viscosity of the fluid;
σ = stress tensor;
ρ = density;
ρ_r = density ratio;
τ = dimensionless time; and
ψ and Ψ = stream function and dimensionless stream function.

Subscript

c = cold;
f = fluid;
h = hot;
i = inner solid cylinder; and
s = solid.

Superscripts

* = dimensional parameters.

1. Introduction

Conjugate heat transfer in enclosures contains heat exchange occurring at the same time by convective heat transfer between a fluid and outer boundary and by conductive heat transfer throughout the solid. The enclosures could be surrounded by solid wall or containing solid obstacles. Essentially, building structures could be handily confined by solid wall. System cooling of electronic components and heat exchangers containing solid

obstacles such as tube, bracket, circuit, electrode and mainboard. There are some excellent subject area considering this structure on fluid circulation and the thermal performance.

House *et al.* (1990) analyzed conjugate heat transfer and studied the influence of heating intensity, fluid type and the obstacle diameter and its conductivity value. They compared the thermal performance of the enclosure with an obstacle and without an obstacle. They conclude that the heat transfer could be enhanced or reduced depending on the obstacle conductivity value. Ha *et al.* (1999) studied the influence of transient natural convection mode in the same configuration. The variation of unsteady heat transfer rate on the bottom hot and top cold walls and at the obstacle surfaces for different heating intensity and thermal boundary conditions are reported by Ha *et al.* (2002). Das and Reddy (2006) studied an enclosure containing a conductive obstacle with different tilted angle. They concluded that the heat transfer rate depends on the orientation angle and of the obstacle conductivity value. Zhao *et al.* (2007) showed that the obstacle conductivity value has strong effect on the fluid circulation in the enclosure. Liu *et al.* (2007) further studied the temperature oscillation on the right wall. They concluded that the resonant frequency of the heat transfer reduces with rising the obstacle dimension and its conductivity value. Mahmoodi and Sebdani (2012) investigated the square enclosure filled with nanoliquid and containing a conductive square obstacle in the middle. They concluded that the thermal performance deteriorated with an increasing of the obstacle dimension for low Rayleigh numbers and enhanced at high Rayleigh numbers. Mahapatra *et al.* (2013) analyzed the conjugate heat transfer and entropy generation in a square enclosure containing insulated or and isothermal obstacles. They obtained the thermal performance enhancement at low heating intensity and beyond a critical solid obstacle dimension. Complete numerical simulation and formulating general concept of the conjugate natural convection in the enclosure by varying the internal object geometry was conducted by Roslan *et al.* (2014). They found that global heat transfer value was not sensitive by changing the obstacles shape. Hu *et al.* (2016) investigated conjugate heat transfer in the enclosure with internal object in multiple configuration. While, Mansour *et al.* (2016) considered the influence of the thermal boundary conditions and magnetohydrodynamics effect on natural convection in a square cavity filled with nanofluid. Recently, Alsabery *et al.* (2018a) filled with the nanoliquids and applied Buongiorno's two-phase model for the liquid layer. They found that the conducting internal object solid allows to shrink the zones of high nanoparticles concentration. Rashad *et al.* (2018) made a numerical investigation of the effects of a heat sink and source size and location on MHD natural convection and entropy generation in an inclined square porous cavity filled with nanofluid. They concluded that a reduction was observed on the convective heat transfer within the porous cavity with an increment of nanoparticle volume fraction. Al-Mudhaf *et al.* (2018) reported the effects of Soret and Dufour on transient natural convection and double diffusive in a porous trapezoidal cavity by using the finite difference method.

Most of the previous subject area on conjugate heat transfer in enclosures with obstacles has considered the wall as rigid. Rapid Developing material technology provides the flexible wall with adjusted elasticities, very thin and various thermal properties. Modeling of actual and real systems may departure sharply from a basic configuration. For example, in building construction elements, the enclosure in the walls is filled with a layer of polyethylene to keep the heat. Other scenario, a very thin membrane layer insulates the sensitive electronic component where the membrane is highly elastic and it deforms through the interaction of the structure with the fluid circulation. Hence, the practical implementation of conjugate natural convection in enclosures with obstacles has encouraged scientist and engineer to analyze the influence of the flexible wall on fluid circulation and heat transfer rate. The present study aims

to examine fluid structure interaction on conjugate heat transfer in enclosure containing a conducting cylinder with a flexible right wall. Research on Fluid-Structure Interaction (FSI) studies of combined convection heat transfer in a lid driven cavity with an elastic bottom surface is conducted by Al-Amiri and Khanafer (2011). They reported that the flexibility of the bottom wall boost the thermal performance. Khanafer (2013) found the heating intensity and the modulus Young value had an intense influence on the wall deformation and consequently produce better thermal performance. Khanafer (2014) concluded that the flexible bottom wall show an improvement of the heat transfer rate compared with a rigid bottom wall.

Selimefendigil and Oztop (2016) reported that the global heat transfer might be increased or decreased depending on the elastic modulus and the Richardson number. Increasing the value of the elastic modulus and nanoparticle concentration is reported by Selimefendigil and Oztop (2017) to increase the heat transfer rate. Selimefendigil *et al.* (2017) obtained significant increasing of the heat transfer rate for the case filling the enclosure with 4 per cent nanoparticle and the magneto hydrodynamics fluid structure model. Mehryan *et al.* (2017a) conducted numerical investigation on the FSI analysis of natural convection heat transfer in an inclined cavity partitioned by a flexible impermeable membrane in the presence of non-uniform temperature. The study of FSI of natural convection heat transfer in a square cavity with an attached flexible horizontal fin was described by Ghalambaz *et al.* (2017). They observed that an increment of the amplitude of the oscillating fin led to a significant enhancement on the convection heat transfer. Recently, Ismael and Jasim (2018) considered the FSI analysis of mixed convection heat transfer in a square vented cavity. They found that the flexible fin showed more enhancement on the average Nusselt number compared to the rigid fin. Zargartalebi *et al.* (2018) made a numerical investigation on the analysis of the fluid-structure interaction of the transient convection flow and heat transfer through a cavity with a flexible thin partition. They concluded that the increasing of the modulus of elasticity led to the maximum non-dimensional stress. Sabbar *et al.* (2018) analyzed the FSI problem of mixed convection heat transfer in a cavity-channel in the presence of flexible wall.

To the best of the authors' knowledge, the unsteady natural convection in an enclosure having a flexible wall and inner solid cylinder has never been reported before. Thus, we believe that this work is valuable. The current study is designed to investigate the fluid structure interaction analysis of conjugate natural convection in a square containing internal solid cylinder and flexible right wall. The main purpose of this numerical work is to investigate the impacts of some parameters such as the Rayleigh number, dimensionless elasticity modulus, dimensionless radius of the solid cylinder and dimensionless length and position of the heat source on the fluid flow and heat transfer characteristics.

2. Mathematical formulation

The 2D transient laminar flow of natural convection for viscous incompressible Newtonian fluid contained in a square cavity with side L and having an inner solid cylinder with radius r is described in Figure 1. The left solid wall of the cavity is partially heated and the remaining parts of the wall are adiabatic, while the right flexible wall is maintained at a constant cold temperature T_c. The horizontal walls are thermally insulated. The thermophysical properties of the fluid are all considered constant, except for the density which obeys the Boussinesq approximation. The Joule-heating effect is neglected. Using the Arbitrary Lagrangian–Eulerian (ALE) formulation, the dimensional governing equations can be written as (Ghalambaz *et al.*, 2017; Alsabery *et al.*, 2018b):

$$\nabla^* \cdot \mathbf{u}^* = 0, \tag{1}$$

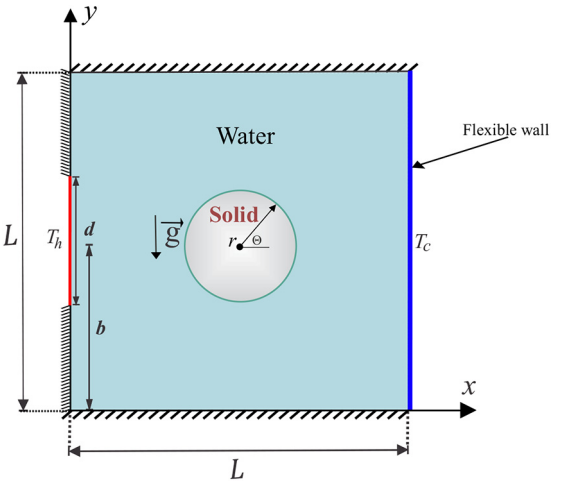

Figure 1.
Physical model of convection in a cavity with a flexible right wall and coordinate system

$$\frac{\partial \mathbf{u}^*}{\partial t} + (\mathbf{u}^* - \mathbf{w}^*) \cdot \nabla^* \mathbf{u}^* = -\frac{1}{\rho_f} \nabla^* P^* + \nu_f \nabla^{*2} \mathbf{u}^* + \beta \vec{g} (T - T_c), \tag{2}$$

$$\frac{\partial T}{\partial t} + (\mathbf{u}^* - \mathbf{w}^*) \cdot \nabla^* T = \alpha_f \nabla^{*2} T. \tag{3}$$

The heat conduction equation in the inner solid cylinder is:

$$\nabla^{*2} T_i = 0. \tag{4}$$

Here **u*** denotes the fluid velocity vector, $\mathbf{w}^* = (u_s^*, v_s^*)$ is the moving coordinate system velocity vector, P^* is the fluid pressure, T is the fluid/solid temperature, ρ_f is the fluid density, ν_f is the kinematic viscosity, α_f and α_s are the thermal diffusivities of the fluid and solid respectively, $\vec{g}$ is the gravitational acceleration, and β is volumetric thermal expansion coefficient.

The structural displacement of the flexible wall is described by Mehryan *et al.* (2017b):

$$\rho_s \frac{d^2 \mathbf{d}_s^*}{dt^2} - \nabla^* \sigma^* = \mathbf{F}_\nu^*, \tag{5}$$

where $\mathbf{d}_s^*$ denotes the solid displacement vector, σ^* represents the stress tensor and $\mathbf{F}_\nu^*$ is the applied body force. The flexible wall is assumed hyper-elastic. The stress tensor in equation (4) is defined using the Neo–Hookean solid model:

$$\sigma^* = J^{-1} F S F^T, \tag{6}$$

where

$$F = \left(I + \nabla^* \mathbf{d}_s^*\right), J = \det(F) \text{ and } S = \frac{\partial W_s}{\partial \varepsilon}, \tag{7}$$

where here T denotes matrix transpose. The strain energy density function W_s and the strain ε are respectively given by:

$$W_s = \frac{1}{2}\mu_l(J - I_l - 3) - \mu_l \ln(J) + \frac{1}{2}\lambda(\ln(J))^2, \tag{8}$$

$$\varepsilon = \frac{1}{2}\left(\nabla^* \mathbf{d}_s^* + \nabla^* \mathbf{d}_s^{*T} + \nabla^* \mathbf{d}_s^{*T} \nabla^* \mathbf{d}_s^*\right), \tag{9}$$

Where $\mu_l = E_\tau/(2(1+v))$ is the Lame second constant and $\lambda = E_v/[(1+v)(1-2v)]$ is the Lame first constant, E_τ the Young modulus, ν Poisson's ratio, and I_l the first invariant of the right Cauchy-Green deformation tensor. At the flexible wall we have the continuity of kinematic forces and dynamic motions:

$$\frac{\partial \mathbf{d}_s^*}{\partial t} = \mathbf{u}^*, \qquad \sigma^* \cdot \mathbf{n} = -P^* + \mu_f \nabla^* \mathbf{u}^*. \tag{10}$$

Assuming there is no energy generation and storage at the flexible wall, the energy equation for the flexible wall can be written as:

$$T = T_c. \tag{11}$$

Upon introducing the dimensionless variables:

$$X = \frac{x}{L},\ Y = \frac{y}{L},\ \mathbf{u} = \frac{\mathbf{u}^* L}{\alpha_f},\ \mathbf{w} = \frac{\mathbf{w}^* L}{\alpha_f},\ \nabla = \frac{\nabla^*}{1/L},\ \nabla^2 = \frac{\nabla^{*2}}{1/L^2},$$

$$\theta = \frac{T - T_c}{T_h - T_c},\ \mathbf{d}_s = \frac{\mathbf{d}_s^*}{L},\ \sigma = \frac{\sigma^*}{E_\tau},\ t_p = \frac{t_p^*}{L},\ \tau = \frac{t\alpha_f}{L^2},\ P = \frac{L^2}{\rho_f \alpha_f^2} P^*,$$

$$\mathbf{F}_\nu = \frac{(\rho_f - \rho_s)Lg}{E_\tau},\ E = \frac{E_\tau L^2}{\rho_f \alpha_f^2},\ Ra = \frac{g\rho_f \beta (T_h - T_c)L^3}{\mu_f \alpha_f},\ \rho_r = \frac{\rho_f}{\rho_s}. \tag{12}$$

We obtain the dimensionless governing equations:

$$\frac{1}{\rho_r}\frac{d^2 \mathbf{d}_s}{d\tau^2} - E\nabla\sigma = E\mathbf{F}_\nu, \tag{13}$$

$$\nabla \cdot \mathbf{u} = 0, \tag{14}$$

$$\frac{\partial \mathbf{u}}{\partial \tau} + (\mathbf{u} - \mathbf{w}) \cdot \nabla \mathbf{u} = -\nabla P + \Pr \nabla^2 \mathbf{u} + \Pr Ra\,\theta, \tag{15}$$

$$\frac{\partial \theta}{\partial \tau} + (\mathbf{u} - \mathbf{w}) \cdot \nabla \theta = \nabla^2 \theta, \tag{16}$$

$$\nabla^2 \theta_i = 0, \tag{17}$$

where $\mathrm{Pr} = \nu_f/\alpha_f$ is the Prandtl number, $\rho_r = \rho_f/\rho_s$ the density ratio and $\alpha_r = \alpha_f/\alpha_s$ thermal diffusivity ratio parameters. In the current work, the influence of the buoyancy force on the flexible right wall is neglected (i.e. $\mathbf{F}_\nu = 0$).

The values of the dimensionless velocity are zero in the solid walls of the cavity. The dimensionless initial and boundary conditions of equations (13)-(17) are:

$$u = v = 0, \ \theta = 0.5, \text{ on the walls of the cavity at } \tau = 0, \tag{18}$$

On the heated part of the left vertical wall:

$$u = v = 0, \ \frac{\partial \theta}{\partial X} = 0, \ X = 0, \ 0 \le Y \le B - (0.5D) \tag{19}$$

On the adiabatic parts of the left wall:

$$u = v = 0, \ \frac{\partial \theta}{\partial X} = 0, \ X = 0, \ 0 \le Y \le B - (0.5D) \text{ and } B + (0.5D) \le Y \le 1, \tag{20}$$

On the right flexible cold wall of the cavity:

$$u = v = 0, \ \theta = 0, \ X = 1, \ 0 \le Y \le 1, \tag{21}$$

On the walls of the inner solid cylinder surface:

$$\theta = \theta_i, \tag{22}$$

$$u = v = 0, \ \frac{\partial \theta}{\partial n} = K_r \frac{\partial \theta_i}{\partial n}, \tag{23}$$

On the adiabatic top and bottom walls of the cavity:

$$\frac{\partial \theta}{\partial Y} = 0, \tag{24}$$

here, n shows the unit vector to the inner solid cylinder. The boundary conditions on the right flexible wall are:

$$\frac{\partial \mathbf{d}_s}{\partial \tau} = \mathbf{u} \text{ and } E\boldsymbol{\sigma} \cdot \mathrm{n} = -P + \mathrm{Pr}\nabla \mathbf{u}. \tag{25}$$

In the present study, the parameter of interest is the Nusselt number, which shows the heat transfer from the wall. The convective heat transfer at the left wall can be written as:

$$q'' = h(T_h - T_c), \tag{26}$$

and the conduction heat transfer at the wall can be written:

$$q'' = -k \frac{\partial T}{\partial x}|_{x=0}. \tag{27}$$

Based on the energy balance at a surface, the conduction heat transfer at the surface equals to the convective heat transfer which yields:

$$h_y(T_h - T_c) = -k\frac{T_h - T_c}{L}\frac{\partial\theta}{\partial X}|_{X=0}. \tag{28}$$

The local Nusselt number at the left wall is written as:

$$Nu_l = -k\frac{h_y L}{k} = -\frac{\partial\theta}{\partial X}|_{X=0}. \tag{29}$$

The average Nusselt number $\overline{Nu_l}$ is achieved by integrating the local Nusselt number at the heated part of the left wall which is given by:

$$\overline{Nu_l} = \int_{B-(0.5D)}^{B+(0.5D)} Nu_l \, \mathrm{d}Y, \tag{30}$$

also, we can calculate the local Nusselt number at the right flexible wall which is written as:

$$Nu_r = -k\frac{h_y L}{k} = -\frac{\partial\theta}{\partial \mathrm{n}}|_{X=0,1}. \tag{31}$$

The average Nusselt number $\overline{Nu_r}$ is achieved by integrating the local Nusselt number at right flexible wall which is given by:

$$\overline{Nu_r} = \int_0^1 Nu_r \mathrm{d}Y, \tag{32}$$

3. Computational methodology and validation

The dimensionless governing equations (13)-(17) subject to the initial and boundary conditions equations (18)-(25) are solved numerically by the Galerkin weighted residual finite element method. The computational domain is discretized into triangular elements as shown in Figure 2. Triangular Lagrange finite elements of different orders are used for each of the flow variables within the computational domain. Residuals for each conservation equation are obtained by substituting the approximations into the governing equations. To simplify the nonlinear terms in the momentum equations, a Newton-Raphson iteration algorithm was used. The details of such a procedure are clearly described in Reddy (1993). The convergence of the solution is assumed when the relative error for each of the variables satisfies the following convergence criteria:

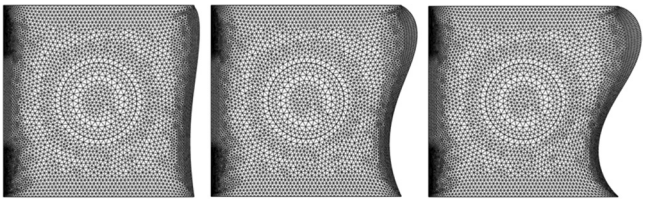

Figure 2.
Grid-points distribution for a grid size 7377

$$\left|\frac{\Gamma^{i+1}-\Gamma^{i}}{\Gamma^{i+1}}\right| \leq \eta,$$

where i represents the iteration number and η is the convergence criterion. In this study, the convergence criterion was set at $\eta = 10^{-6}$. The numerical solution is achieved by computing the Nusselt number for the cavity by using in-house computer code. For the validation of the present work, the results of present study have been compared with the experimental results reported by Nishimura *et al.* (1988) and the numerical results described by Churchill (2002) for natural convection in a cavity with temperature difference at its side walls. The results are depicted in Figure 3 when Pr = 6.0. Also, the result is compared with the earlier published numerical work of Costa and Raimundo (2010) for conjugate natural convection heat transfer in a square cavity with a solid circular cylinder at $Ra = 10^5$, $K_r = 1$ and Pr = 0.7, as described in Figure 4. In addition, another validation is achieved by comparing the average Nusselt number with dimensionless time of the present work with the numerical results of Mehryan *et al.* (2017b) for the case of FSI in natural convection heat transfer within a square cavity equally partitioned by a vertical flexible membrane at $Ra = 10^7$, $E = 10^{14}$, $R = 0$ and Pr = 6.2, as displayed in Figure 5. Based on these validations, it is found that the present result is in a very good agreement with the results of the previously published works.

4. Results and discussion

We present numerical results for the streamlines and isotherms with various dimensionless times ($10^{-8} \leq t \leq 3.5$), Rayleigh number ($10^5 \leq Ra \leq 10^8$), dimensionless elasticity modulus ($10^{12} \leq E \leq 10^{14}$), dimensionless radius of the solid cylinder ($0.1 \leq S \leq 0.4$), dimensionless length of the heat source ($0.2 \leq D \leq 0.8$) and dimensionless position of the heat source ($0.25 \leq B \leq 0.75$). The value of Prandtl number is fixed at Pr = 4.623.

Figure 6 illustrates the transient evolution of the streamlines. Initially, the fluid temperature adjacent to the heater part rises, and the gravitational force help an upward flow above the hot side and the cylinder. This movement creates a clockwise circulation cell. This main cell contains two eye and later, the distant between the eye becomes far away. At the top wall, very small secondary vortices appear due to the presence of the crest in that location. The secondary cell circulation was formed close to the flexible wall. Then, at

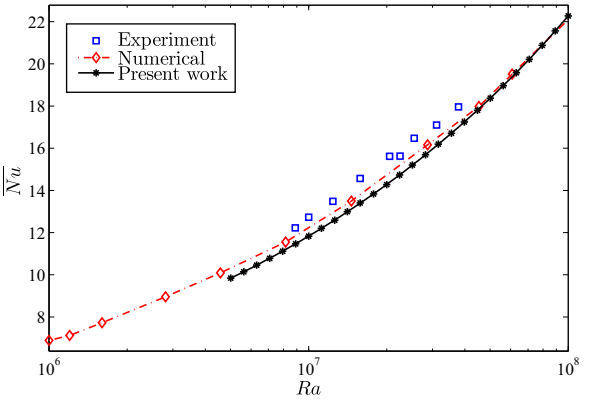

Figure 3.
Comparison between the average Nusselt number of the current numerical work and the experimental data demonstrated by Nishimura *et al.* (1988) and the numerical work based on Churchill's relation by Churchill (2002) with Rayleigh number for a rectangular cavity when $AR = 4$ and Pr = 6

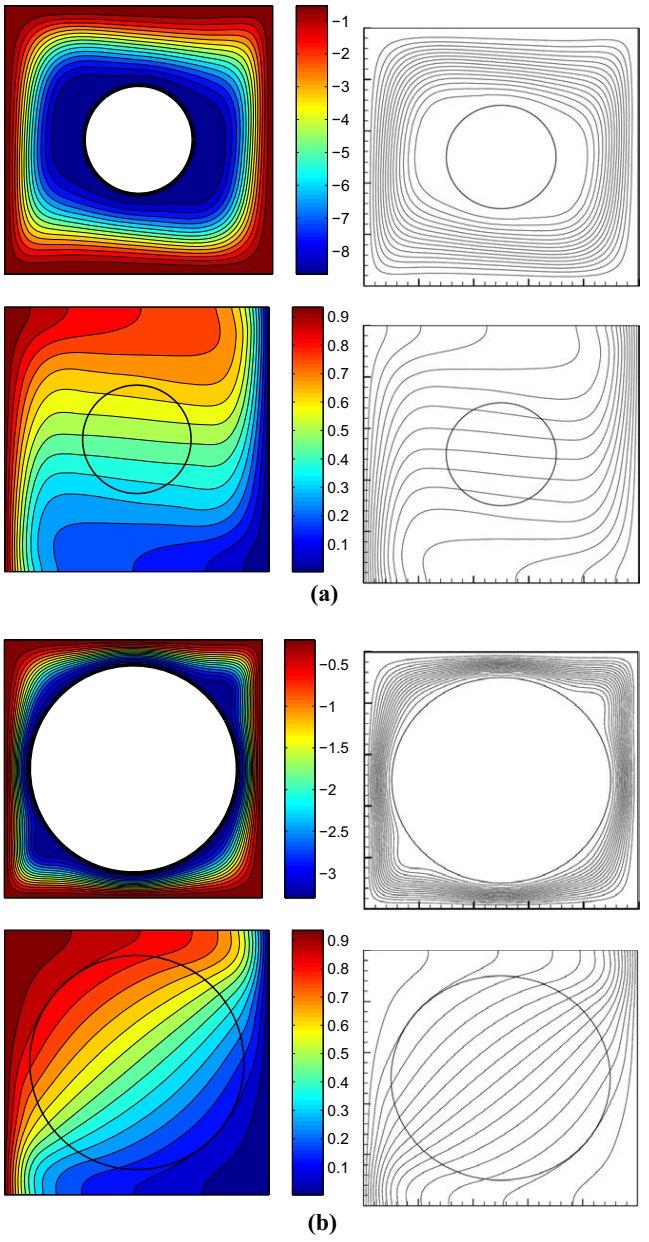

Figure 4.
Streamlines (top) and isotherms (bottom); Costa and Raimundo (2010) (left) and present study (right) for (a) $R = 0.2$ and (b) $R = 0.4$ at $N = 0$, Ra = 10^5, $K_r = 1$ and Pr = 0.7

$t = 10^{-3}$, the secondary circulation strengthen, but later it disappear again at $t = 0.00251$. The secondary circulation was returned at $t = 0.00501$ and its position is pushed to below the cylinder by the flexible wall. The shape of the flexible right wall goes through a semi–monotonic change. The deflection of the flexible wall gets stronger at $t = 0.00813$ and

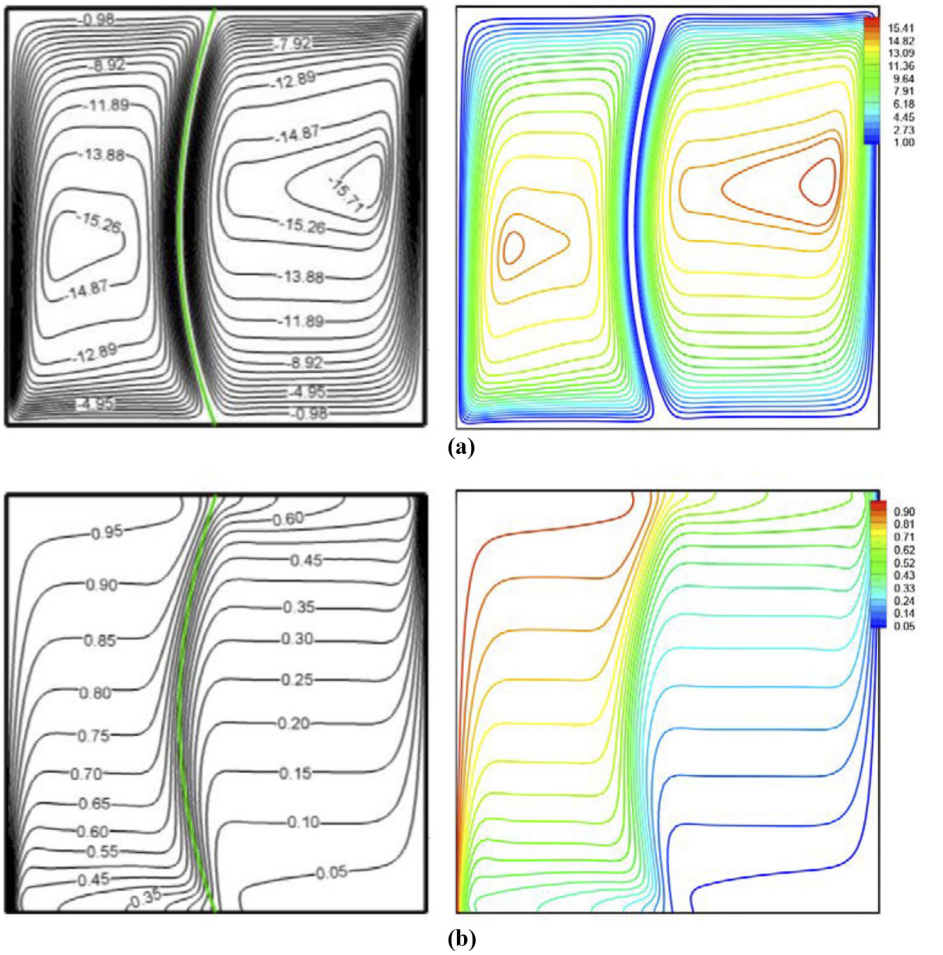

Figure 5.
Streamlines (a), Mehryan *et al.* (2017b) (left), present study (right), isotherms (b), Mehryan *et al.* (2017b) (left), present study (right) for $Ra = 10^7$, $E = 10^{14}$, $R = 0$ and Pr = 6.2

the shape of the main and secondary cells remain unchanging up to $t = 1$. The flexible wall at the top of enclosure is concave while at the bottom is convex, displaying the S shape form. This indicates that the circulations are finally permanent at $t < 1$.

Figure 7 presents the transient evolution of the isotherms. Initially at $t \leq 10^{-3}$, the isotherms spread only above the cylinder. This implies that the heat is transferred only in that region. At $t = 0.00251$ and $t = 0.00501$, the isotherms cross the cylinder and thermal boundary layer was formed in the vicinity of the flexible wall. Later, the heat distributes by convective transportation batch above the cylinder and the inner heat transportation is dominant inside the cylinder. Then, there is no inner heat transportation observed at $t = 0.0251$. At $t = 0.0501$, isotherms are basically vertical near the rigid and flexible walls and horizontal at the middle. It indicates the horizontal heat transport in the neighborhood of the rigid and flexible surfaces and a typical thermal deposition and heat transported oriented vertically at the middle. The isotherms remain unchanging up to $t = 1$. This indicates the

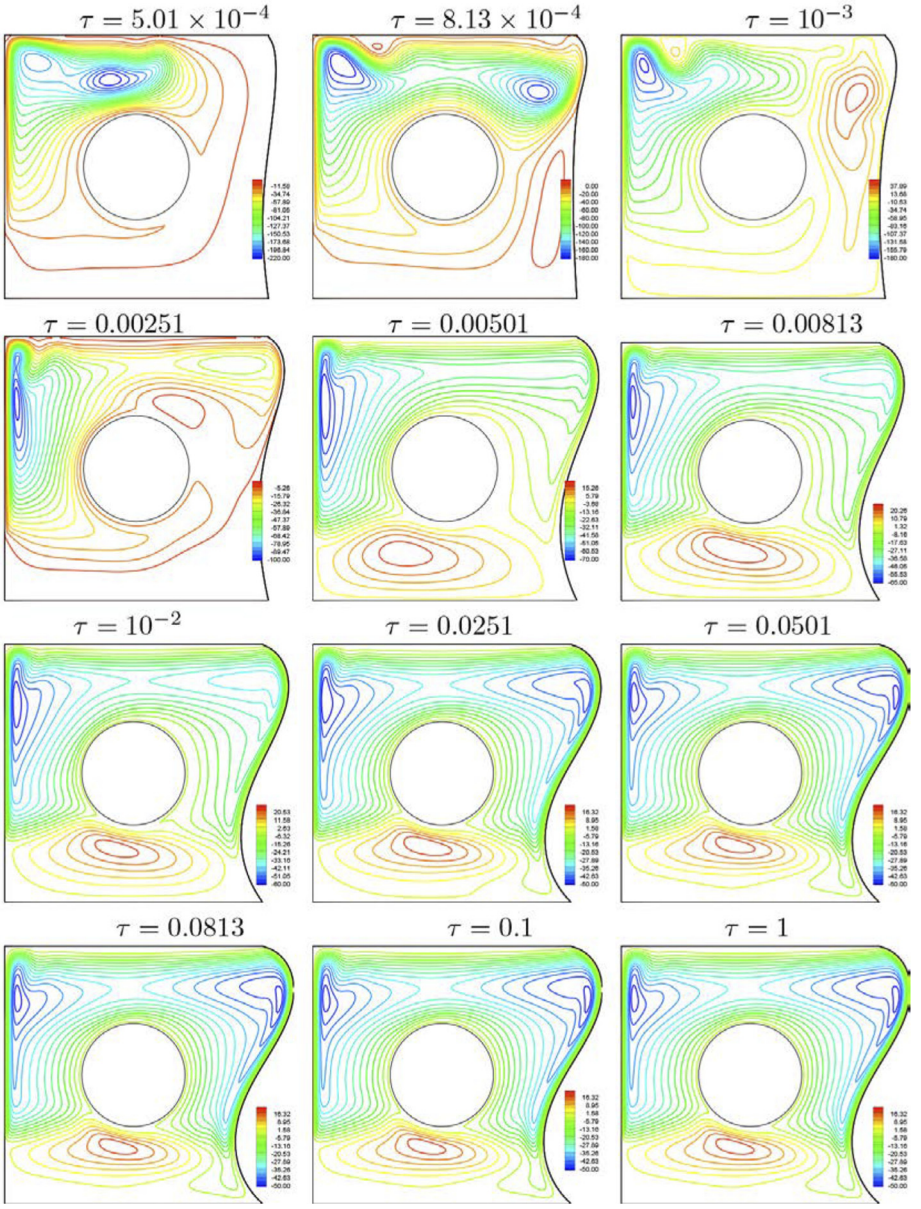

Figure 6.
Streamlines for various dimensionless times (τ) for $Ra = 10^8$, $E = 10^{13}$, $R = 0.2$, $D = 0.5$ and $B = 0.5$

steady, S shape form has achieved somewhere at $t < 1$. This formation is due to the clockwise direction of the natural convection flow.

Figure 8 describes the variation of the streamlines and isotherms evolution by Rayleigh number. Rayleigh number modifies significantly the wall deflection. A small deflection is observed at $Ra = 10^5$ and the deflection gets stronger as the convection intensity gets higher.

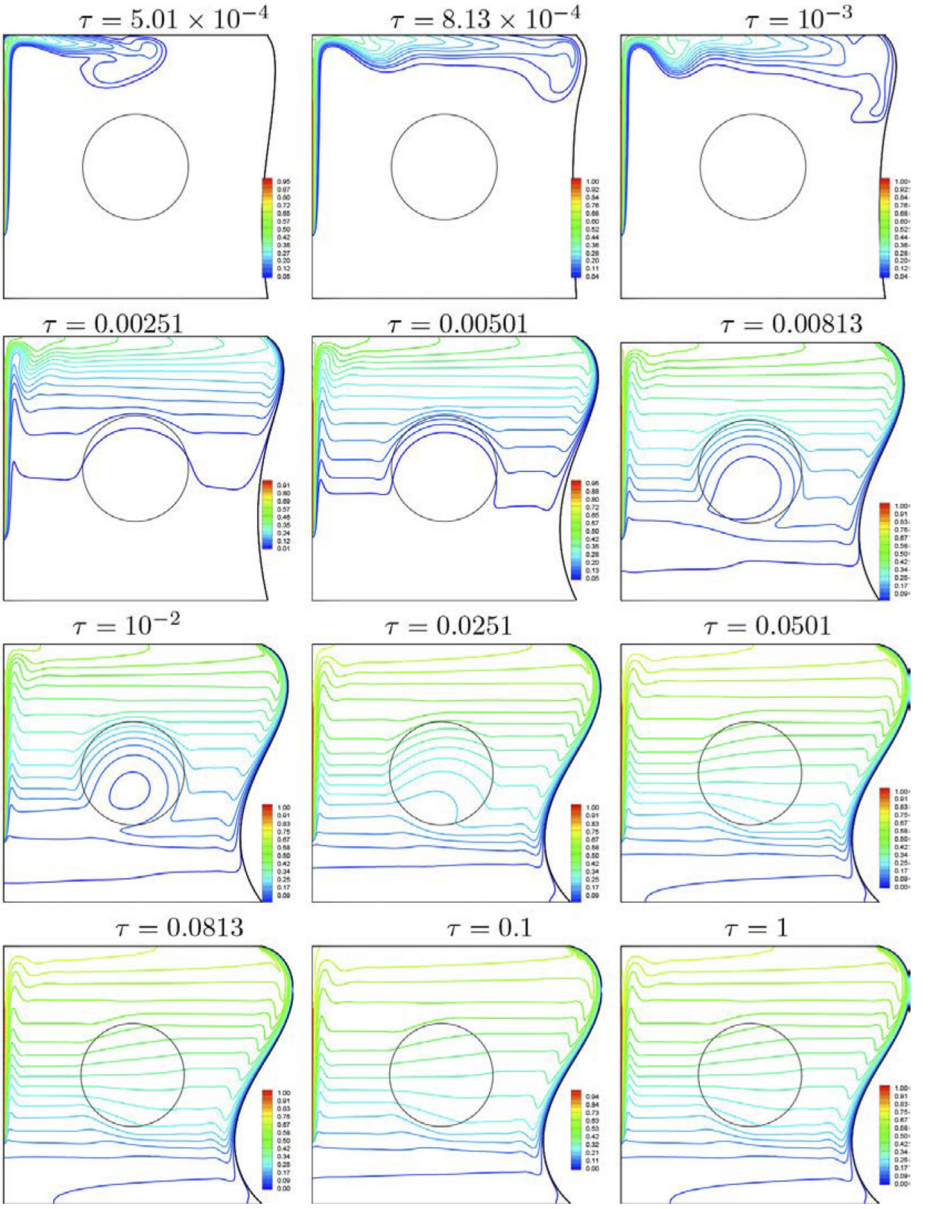

Figure 7.
Isotherms for various dimensionless times (τ) for $Ra = 10^8$, $E = 10^{13}$, $R = 0.2$, $D = 0.5$ and $B = 0.5$

The heated segment brings upward flow, creating main circulation in the center and the downward flow creating secondary circulations close to the bottom and top insulated walls. The big amount of the fluid movement is in the upper region and correspondingly the core of the recirculating eddies is located only in this region. Denser boundary layers at the rigid and flexible walls were formed at $Ra = 10^6$. The secondary cells near the top wall vanish.

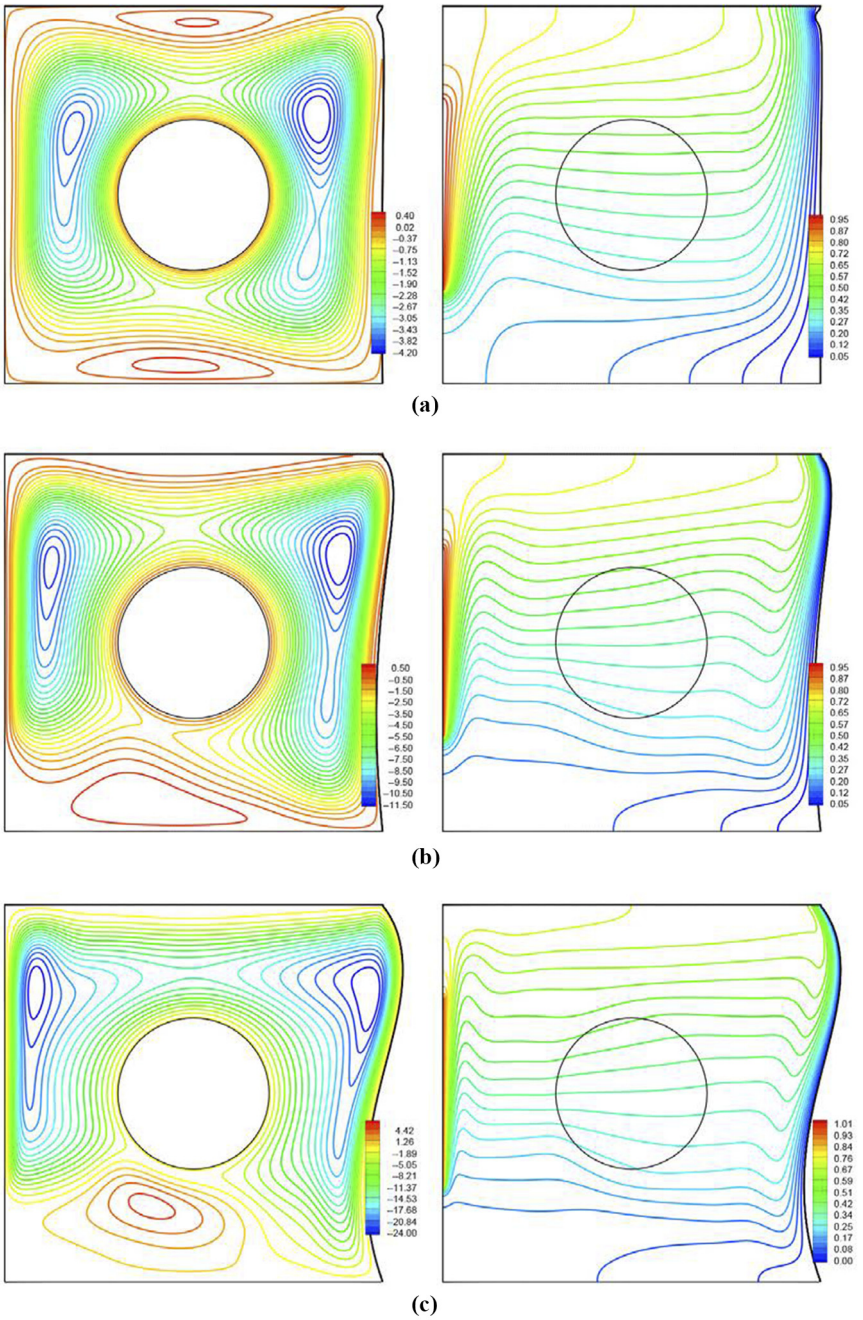

Notes: (a) $Ra = 10^5$; (b) $Ra = 10^6$; (c) $Ra = 10^7$

Figure 8.
Variation of the streamlines (left) and isotherms (right) evolution by Rayleigh number (Ra) for $E = 10^{13}$, $R = 0.2$, $D = 0.5$ and $B = 0.5$

Later at $Ra = 10^7$, the secondary circulation formed below the cylinder becomes stronger and the flexible wall is completely S shape. The cores of the main circulation cells move upward by increasing the Rayleigh number.

Figure 9 display the steady streamlines and steady isotherms evolution by the value of Young's M'odulus. The Modulus Youngs value modifies significantly the wall bending. A large bending, S shape form is observed at $E = 10^{12}$ and the bending gets smaller as the Modulus Youngs value gets higher. It notes that when E goes to infinity the right wall becomes rigid. The main and secondary circulations were observed for the all Young's Modulus value. It seems the shape of the main and secondary cells are almost unaffected by changing the flexibility. Changing the elasticities value do not bring significant different in the heat pattern crossing the cylinder and the free space.

Figure 10 shows the steady streamlines and isotherms evolution by cylinder size. The heated segment brings upward flow, creating main circulation in the center and the contra flow creating secondary circulation close to the insulated wall. The dominant flow is observed in the upper region for $R = 0.2$. It conforms by the fact that the core of the recirculating eddies is located merely in this region. The core of the recirculating eddies is in the upper dan lower parts for $R = 0.3$ and $R = 0.4$. This implies that the dominant flow occurs in that regions. The secondary circulation formed below the cylinder becomes weaker and its core push to the left by growing the cylinder body. At $R = 0.4$, the secondary circulation also appears near the top wall. The horizontal isotherms inside the cylinder body reveal that the heat is transferred vertically within the cylinder in any size. The change in the size of the solid cylinder smoothly changes the steady shape of the flexible wall.

Figure 11 illustrates the streamlines and isotherms evolution by the heater size (D) for $Ra = 10^7$, $E = 10^{13}$, $R = 0.2$ and $B = 0.5$. Double circulation cells were observed above and below the cylinder space. The fluid circulation above the obstacle rotates in the clockwise directions while the smaller cells or secondary circulation below the obstacle rotates in the anti-clockwise direction. The secondary cells shrink by increasing the heater size. Isotherms show different distribution for these localized heating. Denser boundary layer was formed as the heating part is get larger.

Figure 12 demonstrates the streamlines and isotherms evolution by heater location for $Ra = 10^7$, $E = 10^{13}$, $R = 0.2$ and $D = 0.5$. When the heater is located on the upper half part of the enclosure. Elongated vertically Eddies are observed in the case of the lower heater location, $B = 0.45$. The fluid circulation intensity decreases compared with the location in the lower half. The half bottom of the enclosure becomes cooler than the upper half part. There are no isotherms crossing the bottom adiabatic wall at $B = 0.75$.

Figure 13 describes the variation of the steady local Nusselt number on (a) left vertical wall and (b) right flexible right wall for different value of the Modulus Young's. These figures show that the employed Modulus elasticity impacts the distribution of the local Nusselt number in line heated segment of the left wall and the local Nusselt number along the flexible cold wall. The Nusselt number profile at the hot wall exhibits decreasing function by the position and the influence the Modulus Young is not affected the Nu profiles. The Nu profile at the flexible wall exhibits peaks and basins which coincide to the set elasticity values. In addition, the local Nusselt number decreases at the middle of the flexible wall, entering into the fluid domain and increasing along the upper wall protruding out of the domain. It notes that the local heat transfer rate is in the peaks close to the bottom of the cold wall and this is associated with a fact that the clockwise fluid circulation brings heat from the hot wall and it falls then it rises up again. Therefore, the local Nu at the flexible wall decreases as the temperature variation of the fluid and the hot wall decreases.

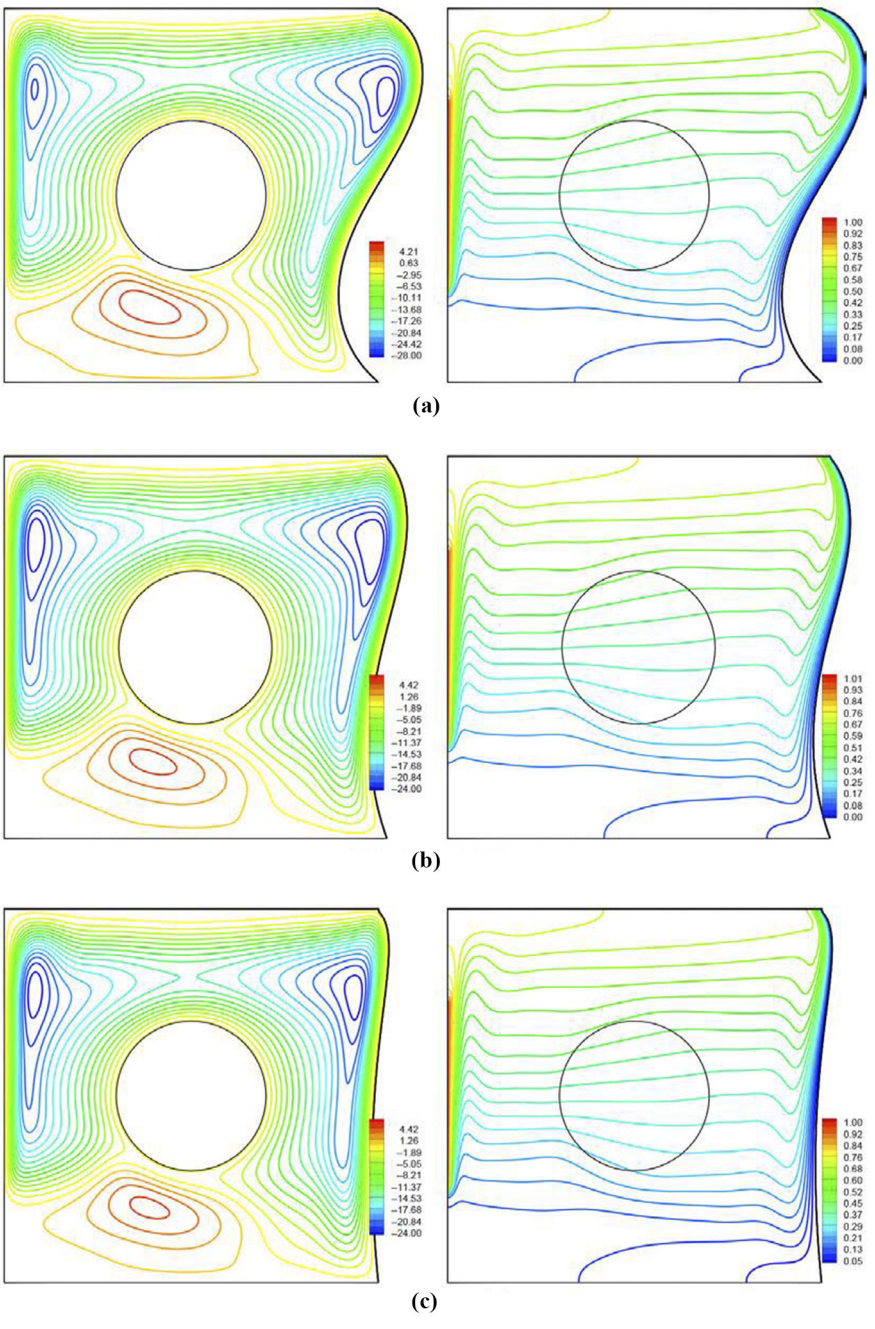

Notes: (a) $E = 10^{12}$; (b) $E = 10^{13}$; (c) $E = 10^{14}$

Figure 9.
Variation of the streamlines (left) and isotherms (right) evolution by Rayleigh number (E) for $Ra = 10^7$, $R = 0.2$, $D = 0.5$ and $B = 0.5$

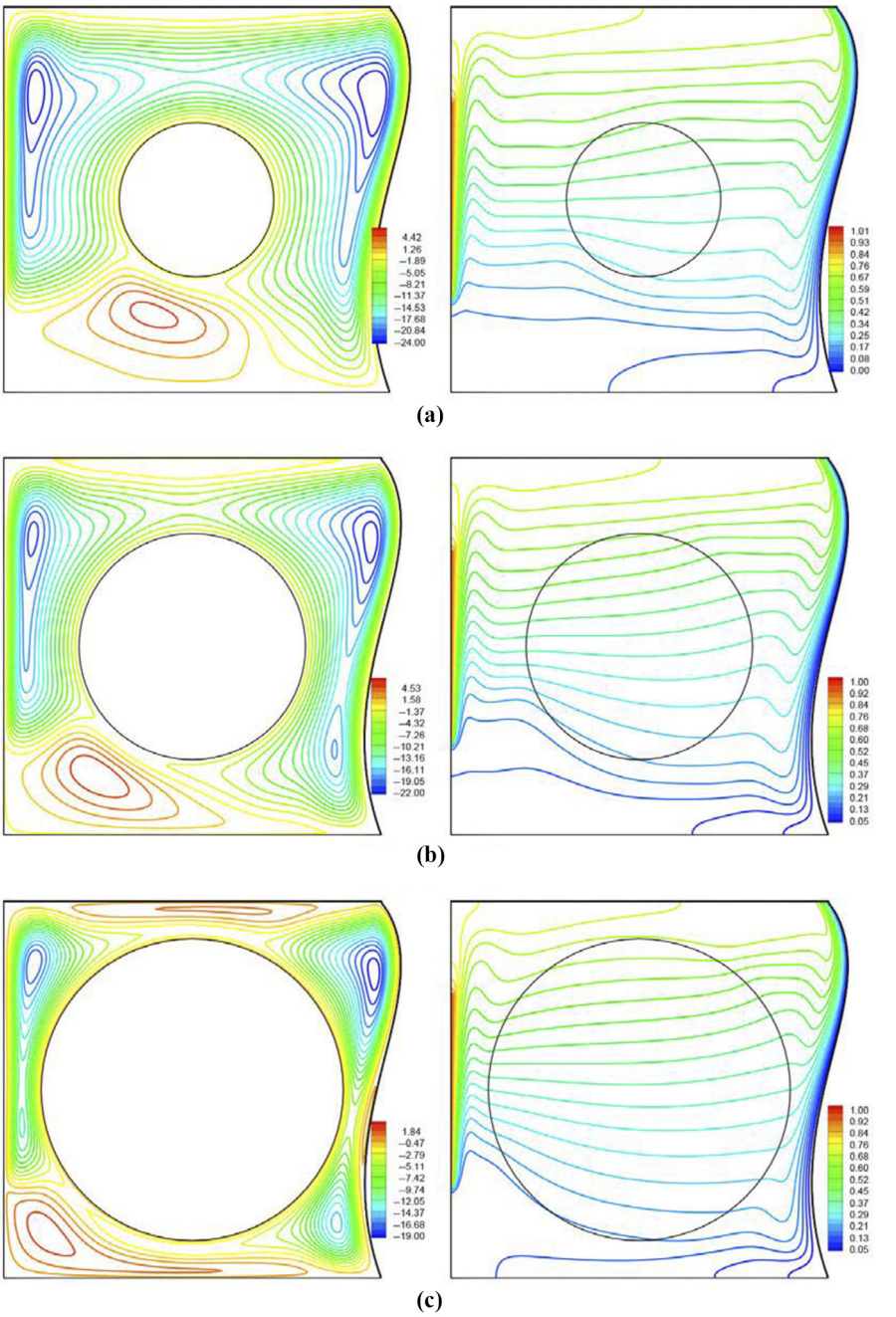

Figure 10.
Variation of the streamlines (left) and isotherms (right) evolution by radius of the solid cylinder (R) for $Ra = 10^7$, $E = 10^{13}$, $D = 0.5$ and $B = 0.5$

Notes: (a) $R = 0.2$; (b) $R = 0.3$; (c) $R = 0.4$

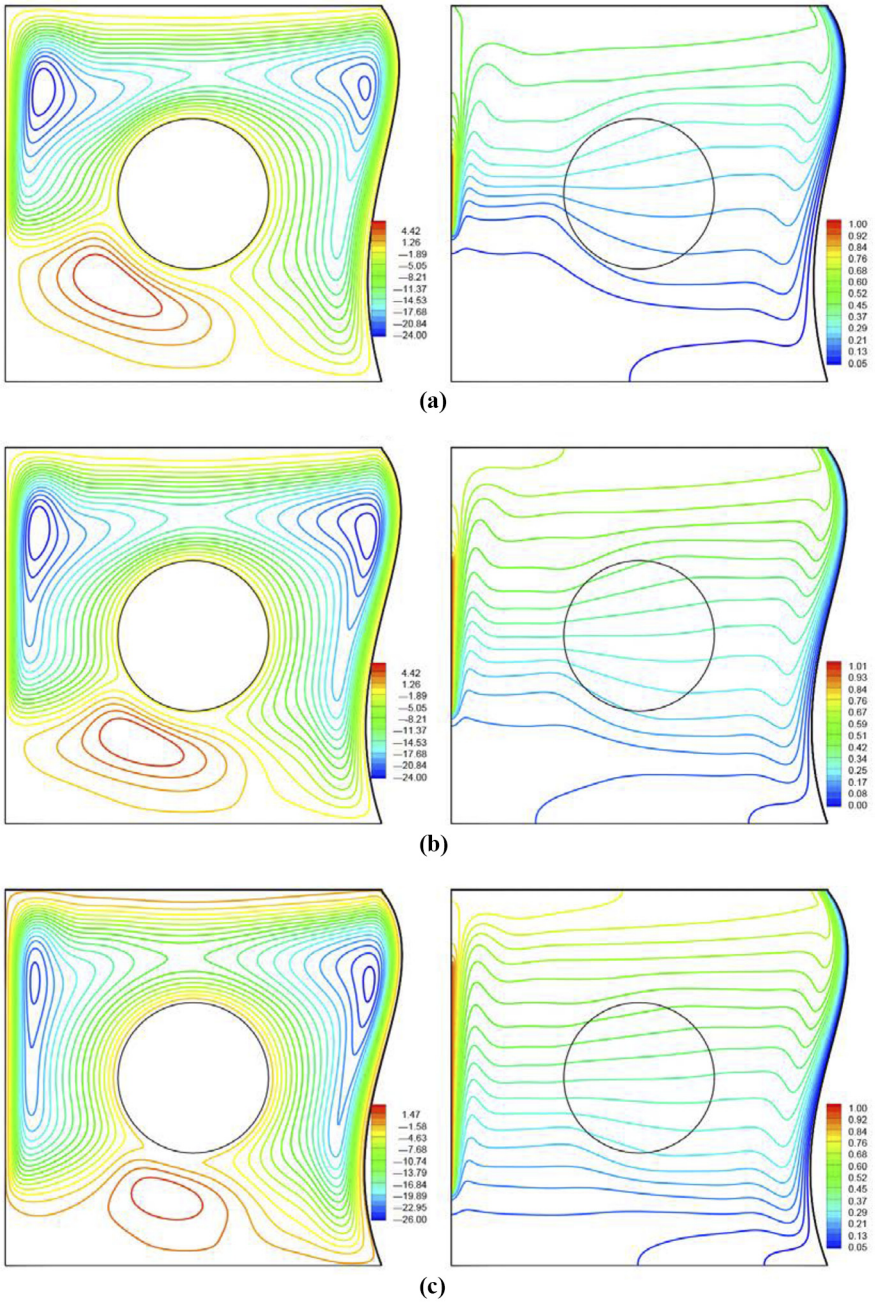

Notes: (a) $D = 0.2$; (b) $D = 0.4$; (c) $D = 0.6$

Figure 11.
Variation of the streamlines (left) and isotherms (right) evolution by length of the heat source (D) for $Ra = 10^7$, $E = 10^{13}$, $R = 0.2$ and $B = 0.5$

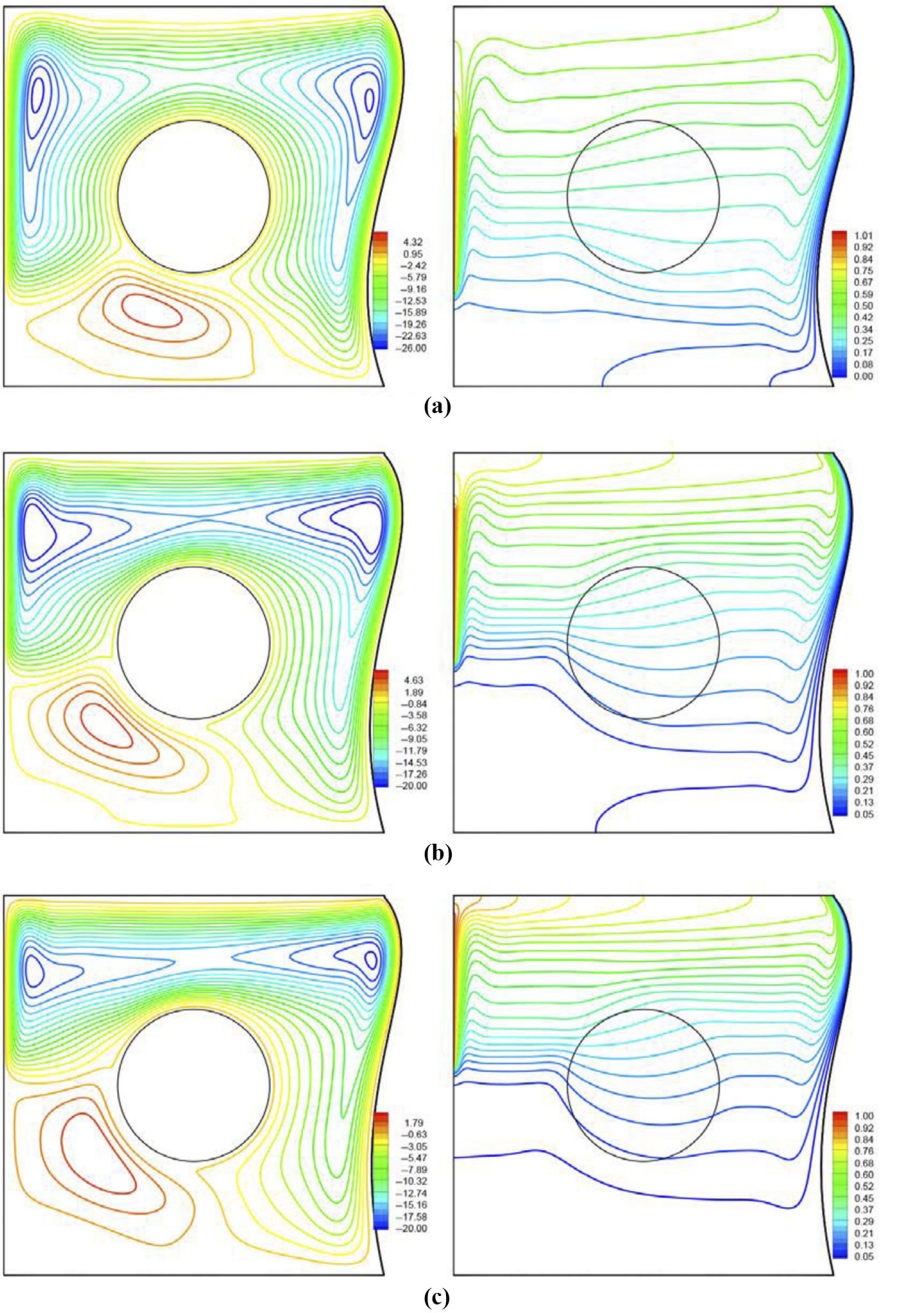

Figure 12.
Variation of the streamlines (left) and isotherms (right) evolution by position of the heat source (B) for $Ra = 10^7$, $E = 10^{13}$, $R = 0.2$ and $D = 0.5$

Notes: (a) $B = 0.45$; (b) $B = 0.65$; (c) $B = 0.75$

Figure 14 presents the fluctuation of the steady local Nusselt number on the right flexible wall for different by varying (a) D and (b) B. The local Nu increases by increasing the heater size. The peaks and valley location are shifted slightly to the left position following the heater size. The peaks and valley location are stagnant by adjusting B from 0.25 to 0.45. The Nusselt number at the lower right wall increases by increasing the B and the Nusselt number at the upper right wall decrease by increasing the B. The left peak location is still static by adjusting B from 0.65 to 0.75 but the right peak and valley location are shifted to the left position when the heater moves upward. Different behavior of the local Nu between the heater location in lower part with the heater location in the upper part was indicated from the fluid circulation in the previous figure.

Figure 15 plots the fluctuation of the steady average Nusselt number on (a) left vertical wall and (b) right flexible wall for different value of Modulus Young's. In

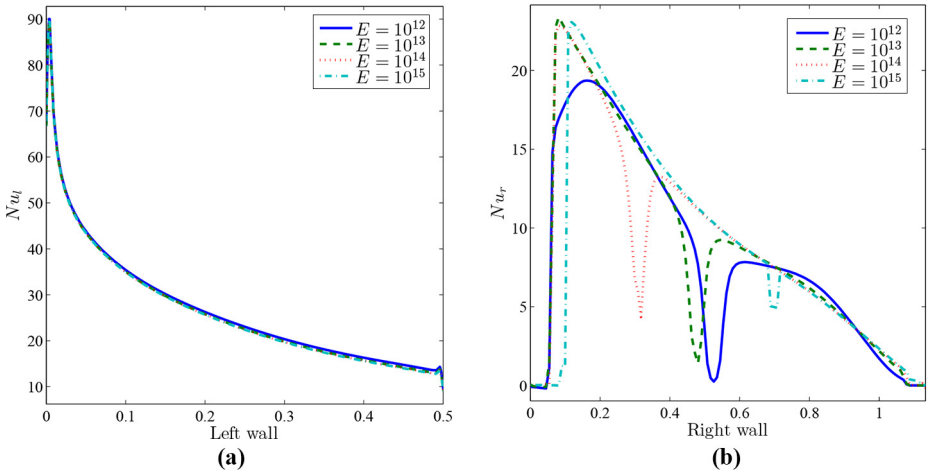

Figure 13. Variation of the steady local Nusselt number on (a) left vertical wall and (b) right flexible right wall for different E at $Ra = 10^7$, $R = 0.2$, $D = 0.5$ and $B = 0.5$

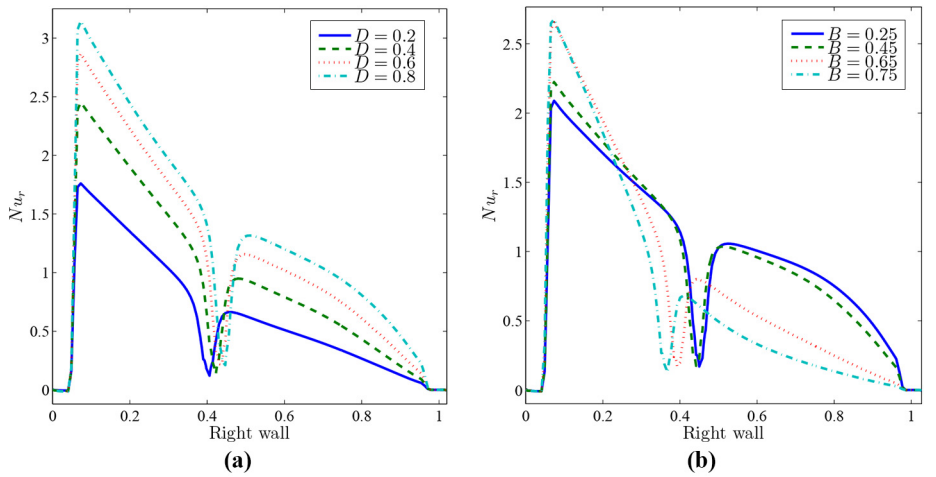

Figure 14. Variation of the steady local Nusselt number on the right flexible right wall for different (a) D and (b) B at $Ra = 10^7$, $E = 10^{13}$ and $R = 0.2$

general, the average Nusselt number at the rigid and flexible walls increases by increasing the Modulus Youngs value at the considered R. In particular, an enhancement in the global heat transfer of the rigid wall for the highest elastic modulus is not effective at the largest cylinder radius. The increase of cylinder size from $R = 0.1$ to $R = 0.25$ increases the average Nusselt number, but further Nu enhancement of R reduce the average Nusselt number. The heat transfer enhancement decreases at higher values of Modulus Young's for $R > 0.375$. In addition, The value of $E = 10^{14}$ can be approximated as a rigid wall. Hence, by reducing E from 10^{14} to 10^{12} the flexibility of the right wall increases and the maximum value of the average Nusselt number at the left hot wall changes from 12.72 to 12.97. This increase in the average Nusselt number of the hot wall is about 2 per cent compared to the rigid wall.

Figure 16 exhibits the variation of the steady average Nusselt number on (a) left vertical wall and (b) right flexible right wall with Ra for different D. Obviously, the heat transfer increases with increasing the convection intensity. In general, the rate of heat transfer at the rigid and flexible walls are enhanced by increasing the heater size. The enhancement is significant at a high Ra value. This fact due to the localized heated has considerable effect when buoyancy force is strong. The heat transfer at the rigid wall slightly decrease by increasing the heater size to $D = 0.8$ at case $Ra = 10^8$.

Figure 17 describes the fluctuation of the steady average Nusselt number on (a) left vertical wall and (b) right flexible right wall with Ra for different heater location. Basically, the Nusselt number at the rigid and flexible walls is enhanced by lowering the heater position. This is due to a sharp collision produced by striking hot fluids

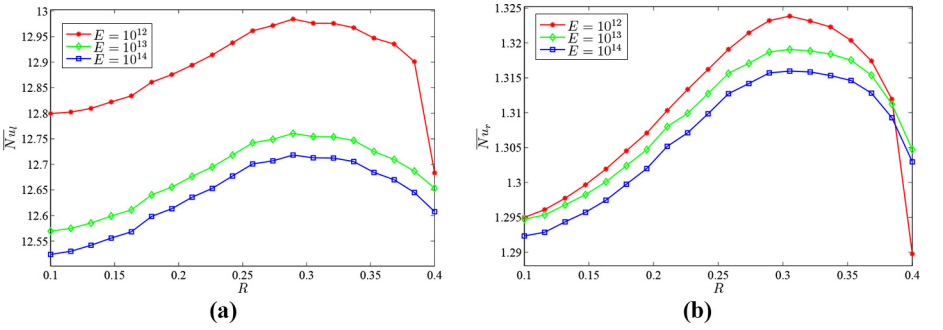

Figure 15.
Variation of the steady average Nusselt number on (a) left vertical wall and (b) right flexible right wall with R for different E at $Ra = 10^7$, $D = 0.5$ and $B = 0.5$

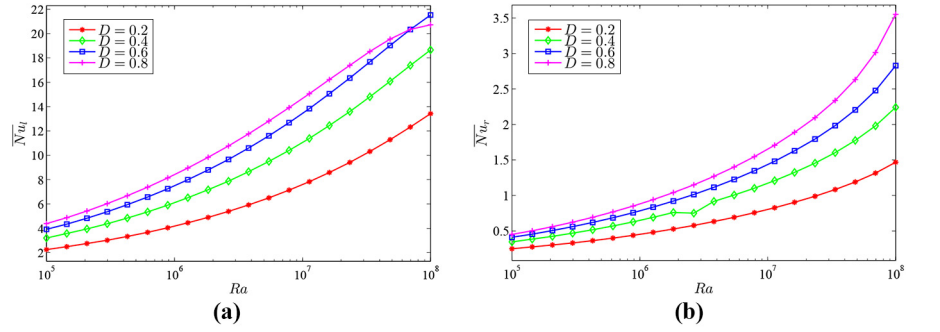

Figure 16.
Variation of the steady average Nusselt number on (a) left vertical wall and (b) right flexible right wall with Ra for different D at $E = 10^{13}$, $R = 0.2$ and $B = 0.5$

against the top adiabatic wall. In this case, the fluid at right bottom corner becomes static due to impingement of rotative fluid to the middle of the hot rigid wall. In addition, the upper half part becomes warmer than the lower half part. Effect of the heater position to the *Nu* enhancement is stronger at higher Rayleigh number.

5. Conclusions

The transient flow and heat transfer in a square cavity with a flexible left cold wall is addressed while there is a fixed solid cylinder in the center of the cavity. The flexible wall under goes through some deformations due to the interaction with the fluid inside the cavity. The change in the shape of the wall constantly changes the cavity shape, and hence, the cavity grids are constantly relocated to maintain their integrity with the new shape of the cavity. Hence, an ALE formulation is utilized in the present study. The governing equations are integrated using the finite element method. The results are reported in the form of contours of the stream lines and isotherms. The graphs for local and average Nusselt number are also reported. The main outcomes of the present study can be summarized as:

- The shape of the flexible right wall goes through a semi-monotonic change until it reaches to its steady S shape form. The flexible wall at the top of the cavity is concave while at the bottom is convex. This formation is due to the clockwise direction of the natural convection flow.
- The increase of the buoyancy effects (the raise of Rayleigh number) boosts the change shape of the flexible wall due to the enhancement of the circulation flow and heat transfer in the cavity. In the case of Ra= 105, the flexible wall is almost smooth. However, in the case of $Ra = 10^7$ the flexible wall is S shape.
- The decrease of the elasticity modulus of the cavity wall also boosts the deformation of the cavity wall. In the case of a rigid flexible wall ($E = 10^{14}$), the flexible wall is almost with no change shape for high values of Ra=107. However, the change shape of the wall at the lower flexibility parameter of $E = 10^{12}$ is quite significant. The increase of the flexibility of the cavity wall enhances the average Nusselt number in the cavity.
- The change in the size of the solid cylinder smoothly changes the final (steady) shape of the flexible wall of the cavity. The increase of the cylinder size from $R = 0.1$ to $R = 0.25$ increases the average Nusselt number, but further increase of R reduces the average Nusselt number.

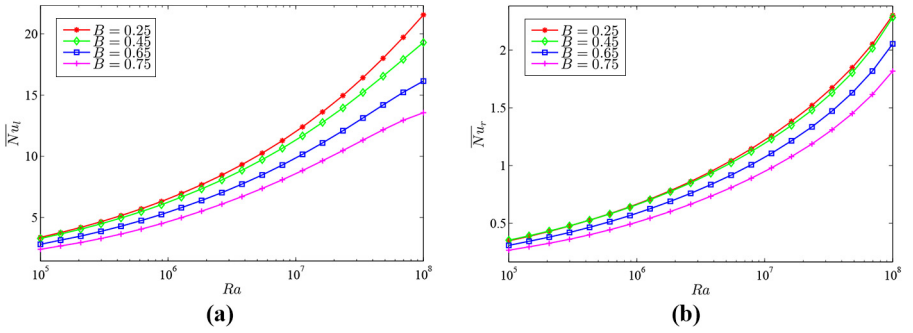

Figure 17. Variation of the steady average Nusselt number on (a) left vertical wall and (b) right flexible right wall with *Ra* for different *B* at $E = 10^{13}$, $R = 0.2$ and $D = 0.5$

References

Al-Amiri, A. and Khanafer, K. (2011), "Fluid-structure interaction analysis of mixed convection heat transfer in a lid-driven cavity with a flexible bottom wall", *International Journal of Heat and Mass Transfer*, Vol. 54 Nos 17/18, pp. 3826-3836.

Al-Mudhaf, A.F., Rashad, A.M., Ahmed, S.E., Chamkha, A.J. and El-Kabeir, S.M.M. (2018), "Soret and Dufour effects on unsteady double diffusive natural convection in porous trapezoidal enclosures", *International Journal of Mechanical Sciences*, Vol. 140, pp. 172-178.

Alsabery, A.I., Sheremet, M.A., Chamkha, A.J. and Hashim, I. (2018a), "Conjugate natural convection of Al_2O_3-water nanofluid in a square cavity with a concentric solid insert using Buongiorno's two-phase model", *International Journal of Mechanical Sciences*, Vol. 136, pp. 200-219.

Alsabery, A.I., Sheremet, M.A., Ghalambaz, M., Chamkha, A.J. and Hashim, I. (2018b), "Fluid-structure interaction in natural convection heat transfer in an oblique cavity with a flexible oscillating fin and partial heating", *Applied Thermal Engineering*, Vol. 145, pp. 80-97.

Churchill, S.W. (2002), "Free convection in layers and enclosures", in Hewitt, G.F. (Ed.), *Heat Exchanger Design Handbook*, Section 2.5.8, Begell House, New York, NY.

Costa, V.A.F. and Raimundo, A. (2010), "Steady mixed convection in a differentially heated square enclosure with an active rotating circular cylinder", *International Journal of Heat and Mass Transfer*, Vol. 53 Nos 5/6, pp. 1208-1219.

Das, M.K. and Reddy, K.S.K. (2006), "Conjugate natural convection heat transfer in an inclined square cavity containing a conducting block", *International Journal of Heat and Mass Transfer*, Vol. 49, pp. 4987-5000.

Ghalambaz, M., Jamesahar, E., Ismael, M.A. and Chamkha, A.J. (2017), "Fluid-structure interaction study of natural convection heat transfer over a flexible oscillating fin in a square cavity", *International Journal of Thermal Sciences*, Vol. 111, pp. 256-273.

Ha, M.Y., Jung, M.J. and Kim, Y.S. (1999), "Numerical study on transient heat transfer and fluid flow of natural convection in an enclosure with a heat-generating conducting body, Numer", *Heat Transf. Part A*, Vol. 35, pp. 415-433.

Ha, M.Y., Kim, I.K., Yoon, H.S., Yoon, K.S., Lee, J.R., Balachandar, S. and Chun, H.H. (2002), "Two-dimensional and unsteady natural convection in a horizontal enclosure with a square body", *Numerical Heat Transfer, Part A*, Vol. 41 No. 2, pp. 183-210.

House, J.M., Beckermann, C. and Smith, T.F. (1990), "Effect of a centered conducting body on natural convection heat transfer in an enclosure", *Numerical Heat Transfer, Part A*, Vol. 18 No. 2, pp. 213-225.

Hu, J.T., Ren, X.H., Liu, D., Zhao, F.Y. and Wang, H.Q. (2016), "Conjugate natural convection inside a vertical enclosure with solid obstacles of unique volume and multiple morphologies", *International Journal of Heat and Mass Transfer*, Vol. 95, pp. 1096-1114.

Ismael, M.A. and Jasim, H.F. (2018), "Role of the fluid-structure interaction in mixed convection in a vented cavity", *International Journal of Mechanical Sciences*, Vol. 135, pp. 190-202.

Khanafer, K. (2014), "Comparison of flow and heat transfer characteristics in a lid-driven cavity between flexible and modified geometry of a heated bottom wall", *International Journal of Heat and Mass Transfer*, Vol. 78, pp. 1032-1041.

Khanafer, K. (2013), "Fluid-structure interaction analysis of non-Darcian effects on natural convection in a porous enclosure", *International Journal of Heat and Mass Transfer*, Vol. 58 Nos 1/2, pp. 382-394.

Liu, D., Zhao, F.Y. and Tang, G.F. (2007), "Conjugate heat transfer in an enclosure with a centered conducting body imposed sinusoidal temperature profiles on one side", *Numerical Heat Transfer, Part A*, Vol. 53 No. 2, pp. 204-223.

Mahapatra, P., De, S., Ghosh, K., Manna, N. and Mukhopadhyay, A. (2013), "Heat transfer enhancement and entropy generation in a square enclosure in the presence of adiabatic and isothermal blocks", *Numerical Heat Transfer, Part A*, Vol. 64 No. 7, pp. 577-596.

Mahmoodi, M. and Sebdani, S.M. (2012), "Natural convection in a square cavity containing a nanofluid and an adiabatic square block at the center", *Superlattices and Microstructures*, Vol. 52 No. 2, pp. 261-275.

Mansour, M.A., Ahmed, S.E. and Rashad, A.M. (2016), "MHD natural convection in a square enclosure using nanofluid with the influence of thermal boundary conditions", *Journal of Applied Fluid Mechanics*, Vol. 9.

Mehryan, S.A.M., Chamkha, A.J., Ismael, M.A. and Ghalambaz, M. (2017a), "Fluid-structure interaction analysis of free convection in an inclined square cavity partitioned by a flexible impermeable membrane with sinusoidal temperature heating", *Meccanica*, Vol. 52 Nos 11/12, pp. 2685-2703.

Mehryan, S., Ghalambaz, M., Ismael, M.A. and Chamkha, A.J. (2017b), "Analysis of fluid-solid interaction in MHD natural convection in a square cavity equally partitioned by a vertical flexible membrane", *Journal of Magnetism and Magnetic Materials*, Vol. 424, pp. 161-173.

Nishimura, T., Shiraishi, M., Nagasawa, F. and Kawamura, Y. (1988), "Natural convection heat transfer in enclosures with multiple vertical partitions", *International Journal of Heat and Mass Transfer*, Vol. 31 No. 8, pp. 1679-1686.

Rashad, A.M., Armaghani, T., Chamkha, A.J. and Mansour, M.A. (2018), "Entropy generation and MHD natural convection of a nanofluid in an inclined square porous cavity: effects of a heat sink and source size and location", *Chinese Journal of Physics*, Vol. 56 No. 1, pp. 193-211.

Reddy, J.N. (1993), *An Introduction to the Finite Element Method*, Vol. 2, McGraw-Hill, New York, NY,

Roslan, R., Saleh, H. and Hashim, I. (2014), "Natural convection in a differentially heated square enclosure with a solid polygon", *The Scientific World Journal*, Vol. 2014.

Sabbar, W.A., Ismael, M.A. and Almudhaffar, M. (2018), "Fluid-structure interaction of mixed convection in a cavity-channel assembly of flexible wall", *International Journal of Mechanical Sciences*, Vol. 149, pp. 73-83.

Selimefendigil, F. and Oztop, H. (2016), "Analysis of MHD mixed convection in a flexible walled and nanofluids filled lid-driven cavity with volumetric heat generation", *International Journal of Mechanical Sciences*, Vol. 118, pp. 113-124.

Selimefendigil, F. and Oztop, H. (2017), "Mixed convection in a partially heated triangular cavity filled with nanofluid having a partially flexible wall and internal heat generation", *Journal of the Taiwan Institute of Chemical Engineers*, Vol. 70, pp. 168-178.

Selimefendigil, F., Oztopztop, H. and Chamkha, A. (2017), "Fluid-structure-magnetic field interaction in a nanofluid filled lid-driven cavity with flexible side wall", *European Journal of Mechanics, B/Fluids*, Vol. 61, pp. 77-85.

Zargartalebi, H., Ghalambaz, M., Chamkha, A., Pop, I. and Nezhad, A.S. (2018), "Fluid-structure interaction analysis of buoyancy-driven fluid and heat transfer through an enclosure with a flexible thin partition", *International Journal of Numerical Methods for Heat and Fluid Flow*, Vol. 28, pp. 2072-2088.

Zhao, F.Y., Liu, D. and Tang, G.F. (2007), "Conjugate heat transfer in square enclosures", *Heat and Mass Transfer*, Vol. 43 No. 9, pp. 907-922.

Author affiliations

Ammar I. Alsabery, Refrigeration and Air-Conditioning Technical Engineering Department, College of Technical Engineering, The Islamic University, Najaf, Iraq and Centre for Modelling and Data Science, Faculty of Science and Technology, Universiti Kebangsaan Malaysia, Bangi, Selangor, Malaysia

Habibis Saleh, Mathematics Education Department, Universitas Islam Negeri Sultan Syarif Kasim Riau, Pekanbaru, Indonesia

Mohammad Ghalambaz, Department for Management of Science and Technology Development, Ton Duc Thang University, Ho Chi Minh City, Vietnam and Faculty of Applied Sciences, Ton Duc Thang University, Ho Chi Minh City, Vietnam

Ali J. Chamkha, Department of Mechanical Engineering, Prince Sultan Endowment for Energy and the Environment, Prince Mohammad Bin Fahd University, Al-Khobar, Saudi Arabia and RAK Research and Innovation Center, American University of Ras Al Khaimah, Ras Al Khaimah, United Arab Emirates

Ishak Hashim, Centre for Modelling and Data Science, Faculty of Science and Technology, Universiti Kebangsaan Malaysia, Bangi Selangor, Malaysia

Corresponding authors

Ammar I. Alsabery can be contacted at: ammar_e_2011@yahoo.com and Mohammad Ghalambaz can be contacted at: mohammad.ghalambaz@tdtu.edu.vn